

Electronic energy transfer from metastable argon atoms to krypton atoms

L. G. Piper and D. W. Setser

Department of Chemistry, Kansas State University, Manhattan, Kansas 66506

M. A. A. Clyne

Department of Chemistry, Queen Mary College, Mile End Road, London, E1, United Kingdom

(Received 4 August 1975)

The interaction between metastable argon atoms ($^3P_{2,0}$) and krypton atoms has been studied at room temperature using the flowing afterglow technique. Measurements of the emission intensities from the excited-krypton levels show that only $Kr(5p[3/2]_2)$ and $Kr(5p[3/2]_1)$ are primary products from $Ar^*(^3P_2)$. The pressure dependence of the emission intensities from other $5p$ krypton states shows that these are produced by collisional cascade from the $5p[3/2]_{2,1}$ levels; some rate constants for these cascade processes are reported. Absorption measurements using the 123.6 nm resonance transition of Kr demonstrate that the emitting $Kr(5s^3P_1)$ state carries no excess translational energy; therefore, it must be produced only via radiative cascade from $Kr(5p)$ levels. Thus $Ar(^3P_2)$ excitation rate constants of 5.6 and $0.65 \times 10^{-12} \text{ cm}^3 \text{ molecule}^{-1} \text{ sec}^{-1}$ are established for excitation to $Kr(5p[3/2]_2)$ and $Kr(5p[3/2]_1)$, respectively. The $Ar(^3P_2) + Kr$ reaction can serve as a reference for obtaining rate constants for excitation of other species via comparison of relative emission intensities and the technique is even useful in the vacuum ultraviolet if the appropriate branching ratio for the radiative cascade from $5p[3/2]_{2,1}$ to $Kr(5s^3P_1)$, established here as 0.301 ± 0.006 , is utilized. The emission from Kr^* also can serve as a reference for determining absolute emission rates if $[Ar(^3P_2)]$, $[Kr]$, and the emission intensities are simultaneously measured. Quenching of $Ar(^3P_0)$ by Kr gave an Ar-Kr* excimer emission, which peaks around 756.5 nm, emission from $Kr(5p[1/2]_0)$ at 758.7 nm, and formation of lower $Kr(5p)$ states or deactivation to lower $Ar(4s)$ states. Based upon the pressure dependence of these emission intensities, the excimer is formed by a fast three-body reaction with $Ar^*(^3P_0)$, and $Kr(5p[1/2]_0)$ is excited both by a slow two-body reaction with $Ar(^3P_0)$ ($\sim 3.4 \times 10^{-15} \text{ cm}^3 \text{ molecule}^{-1} \text{ sec}^{-1}$) and by bimolecular quenching of the excimer.

I. INTRODUCTION

A comprehensive program¹⁻⁴ directed to measurement of the total quenching rate constants and assignment of branching ratios to product channels from quenching of the first-excited (metastable) states of the rare gas atoms is in progress in our laboratories. We previously reported the rate constants for quenching metastable argon atoms by Xe,^{2a} Kr,^{2b} O³ atoms as well as the rate constants for quenching of both argon and xenon metastables by a variety of small molecules.² In this paper, the product channels from the interaction of metastable-argon atoms ($^3P_{0,2}$) with krypton are identified and the formation rate constants for the primary excitation channels are obtained. The quantum states of both product and reactant channels are specified for the $Ar(^3P_2) + Kr$ reaction, and the system can be discussed within the limitations of available theory. Furthermore, the $Ar(^3P_2) + Kr$ reaction provides a primary reference rate constant that permits easy measurement of product channel rate constants for other excitations from reagents that yield emissions from interaction with $Ar(^3P_2)$.

In addition to the primary quenching processes, secondary collisional quenching of the excited product states of krypton by the argon bath gas was observed in the 1-6 torr region. In favorable cases, rate constants for the collisional relaxation of the excited Kr states were estimated.

Experiments consist of observation of emission from krypton states in a flowing-afterglow apparatus follow-

ing addition of a flow of Kr downstream from the discharge source which generates the metastable argon atoms. The excitation of krypton via energy transfer from metastable-argon atoms can be observed directly. The relative Kr emission intensities permit the total rate constant² to be partitioned into formation rate constants for individual product channels. A kinetic-energy balance of the reaction was obtained by resonance-absorption measurements using the $5s^3P_1 - ^1S_0$ transition (123.6 nm) from the $Ar(^3P_2) + Kr$ reaction as the source of the resonance radiation. Since the $5p[3/2]_{1,2}$ levels of Kr have nearly the same energy as $Ar(^3P_2)$, no significant broadening of the resonance line is expected if the $Kr(5s, ^3P_1)$ level is produced by radiative cascade. The results of resonance absorption experiments were fully consistent with a 300 °K Doppler line shape for the resonance line. Thus, no detectable direct excitation of $Kr(5s^3P_1)$ from $Ar(^3P_2)$ occurred, and the $Kr(5s^3P_1)$ state is produced only via radiative cascade from the $Kr(5p)$ levels, which are initially produced by the $Ar(^3P_2) + Kr$ reaction.

Bochkova⁵ studied the product channels for excitation of Kr by metastable argon in a static discharge and over a limited spectral range. Although Bochkova did not take collisional quenching of $Kr(5p)$ levels into account and her data are not properly weighted by the appropriate transition probabilities, her cross sections fortuitously agree with ours. In a recent molecular-beam study of the elastic scattering of metastable argon by krypton, Winicur and Fraites⁶ observed an enhancement of the scattered metastable signal at large angles. This

enhancement was assumed to result from metastable krypton atoms formed from the exchange of electronic energy between $\text{Ar}(^3P_{0,2})$ and Kr. Winicur and Fraitess⁶ obtained cross sections for the formation of metastable Kr atoms and an analysis of the kinetic energy of the products. The molecular-beam results basically are in agreement with the data reported here.

The coupling scheme for excited rare-gas atomic states is best⁷ described by j_c-l coupling, in which the l and s of the core are strongly coupled and the resultant j_c then is coupled to the l of the excited electron. A prime is used to designate the higher energy (lower j_c) of the two core-coupling cases. In the more familiar $L-S$ notation, the argon metastable states are 3P_2 (11.548 eV) and 3P_0 (11.723 eV). This designation will be retained for the $\text{Ar}(4s)$ and $\text{Kr}(5s)$ states, but the j_c-l notation will be used to describe the $\text{Kr}(5p)$ states, where the coupling is more nearly of this type.

II. EXPERIMENTAL

The apparatus employed for these studies was a discharge-flow reactor, similar to those used previously.¹ Argon, purified by passage through a 77 °K molecular-sieve trap at low pressure, flowed through a hollow-cathode, dc discharge (200 V, ~1 mA) which converts some of the argon atoms to the metastable states. The discharged argon subsequently flowed through two right-angle light traps to eliminate resonance states of argon and to reduce scattered light, and then into the observation region of the flow tube; the ratio of $\text{Ar}(^3P_2)$ to $\text{Ar}(^3P_0)$ at the observation zone is ~9. Krypton atoms entered the observation region coaxially with the flow of argon metastables and the two species were mixed by diffusion. Spectral observations were made normal to the gas flow. Observations in the infrared (750–850 nm) were made with a calibrated, 0.75 m, Jarrell-Ash, Czerny-Turner scanning monochromator equipped with a photon-counting rate meter and a photomultiplier tube (EMI 9558Q). The quantum efficiency of the monochromator plus detector was obtained from a standard lamp; it was checked by observing several nonreversed^{2b} argon emission lines (from a pen-ray lamp)^{2b} originating from a common level. The observed relative intensities agreed with known branching ratios of the Einstein coefficients.^{7b} The observed Kr emission lines were assigned according to Kaufman and Humphries,^{7a} and the intensities of the transitions were measured as peak heights (or when necessary as integrated areas) on a strip-chart recorder.

The vacuum ultraviolet studies were undertaken with a standard metastable-argon flow cell, but with a second flow tube (absorption cell) placed between the metastable cell and a 1 m normal-incidence monochromator (Hilger & Watts E760). LiF windows separated the two flow tubes and also separated the absorption flow tube from the monochromator. Light was detected with a sodium salicylate phosphor and a photomultiplier tube (EMI 9789QA) operated in the pulse-counting mode.

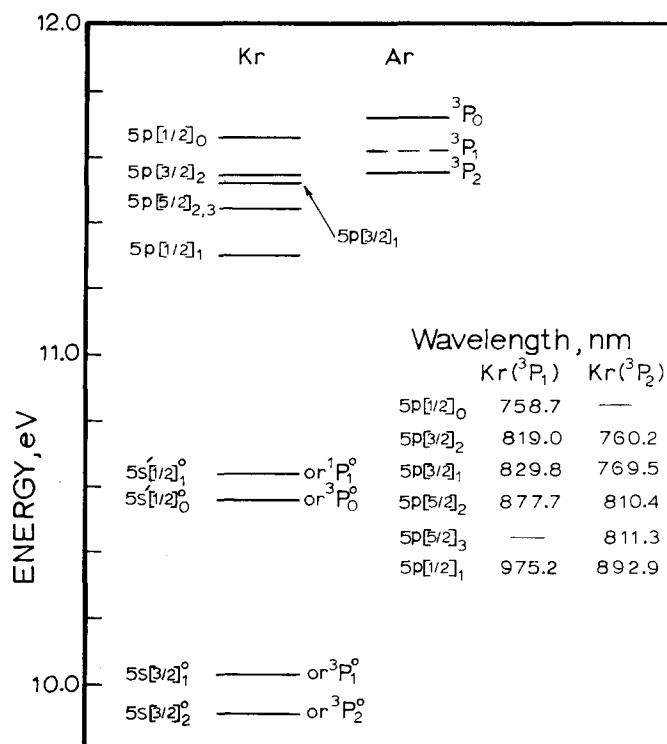


FIG. 1. Energy levels for Ar and Kr and the wavelengths of the transitions between the $\text{Kr}(5p)$ states and the $\text{Kr}(5s)$ states. The upper $\text{Ar}(^1P_1)$ resonance level (11.82 eV) is not shown on the diagram; the lower energy resonance level is denoted by the dotted line.

III. RESULTS

A. Excitation by $\text{Ar}^*(^3P_2)$

Figure 1 shows the states of krypton which are accessible by collision with $(\text{Ar}^3P_{0,2})$ and the wavelengths of the radiative transitions connecting the different levels.^{7a} Our observations showed that the primary excitation of Kr by $\text{Ar}(^3P_2)$ was into the $5p[3/2]_2$ and $5p[3/2]_1$ states. Since all important transitions from these two states were observed, the sum of intensities from a given state was directly proportional to its population. The relative populations of the krypton levels were mildly pressure dependent (see Figs. 2 and 3), and at higher pressures emission was observed from the $5p[5/2]_2$ (11.444 eV) and the $5p[5/2]_3$ (11.443 eV) states. Since the emission intensities from the $[5/2]_{2,3}$ levels extrapolate to zero at zero pressure (Fig. 3), these levels must be produced by collision from the $5p[3/2]_2$ and $5p[3/2]_1$ levels. Emission at 892.9 nm, which would indicate the presence of $\text{Kr}(5p[1/2]_1)$, was not observed. In order to detect this emission with our apparatus, the population of the $5p[1/2]_1$ level would have to exceed that of $5p[3/2]_2$ by about a factor of 5. Since the $5p[5/2]_{2,3}$ levels were populated only by collisional cascade from the $5p[3/2]_1$ level, it is unlikely that direct excitation by $\text{Ar}^*(^3P_2)$ of the $5p[1/2]_1$ level would have occurred.

Extrapolation of the $5p[3/2]_2$ to $5p[3/2]_1$ population ratio to zero pressure (Fig. 4) gives an intercept value of 8.6 ± 0.4 , and $89.5 \pm 0.5\%$ of the excitation is to the $5p[3/2]_2$ level. Based upon excitation of Kr as being the only

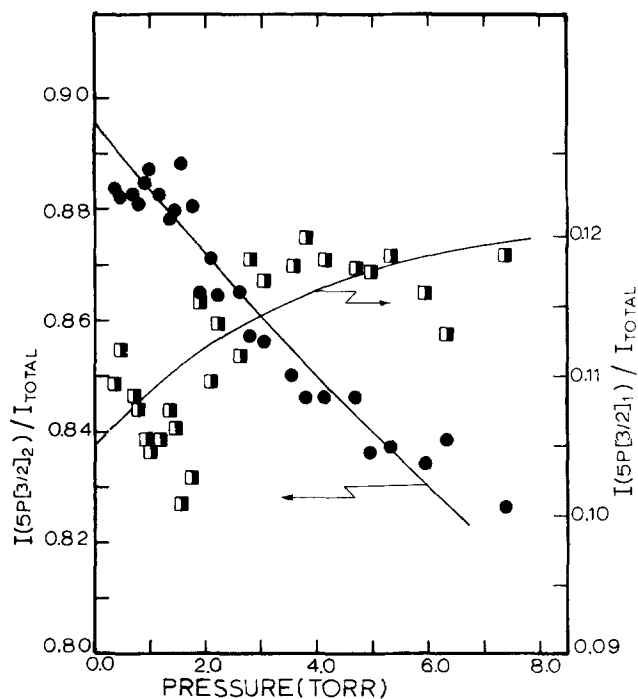


FIG. 2. The fraction of the total krypton emission intensity excited by $\text{Ar}^*(^3P_2)$ emanating from the $\text{Kr}(5p[3/2]_2)$ (\bullet) and $\text{Kr}(5p[3/2]_1)$ (\blacksquare) levels as a function of pressure. The lines through the data are derived from a least-square computer fit to the kinetic scheme discussed in the text.

quenching pathway, the rate constants^{2a} (cross sections) are $5.6 \times 10^{-12} \text{ cm}^3 \text{ sec}^{-1}$ (1.16 \AA^2) for excitation of $5p[3/2]_2$

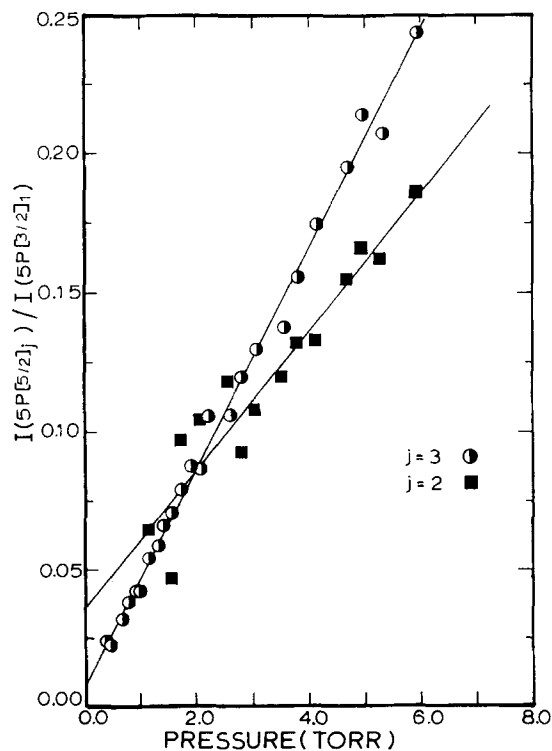


FIG. 3. The ratio of emission intensity from the $5p[5/2]_2$ (\blacksquare) and $5p[5/2]_3$ (\bullet) levels to that from the $5p[5/2]_1$ level. The solid lines are least squares fits to the kinetic scheme discussed in the text.

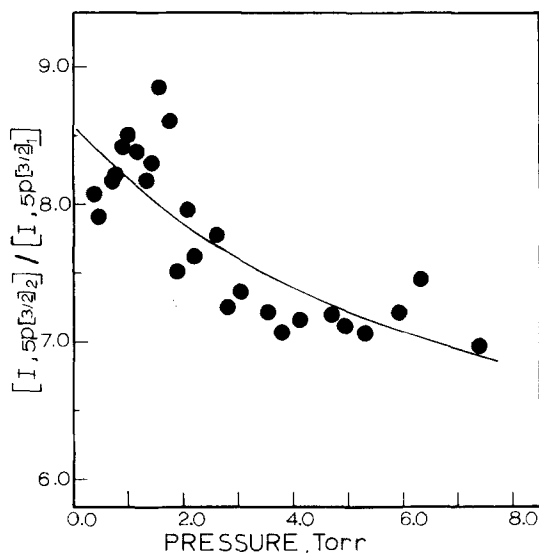


FIG. 4. The ratio of emission intensities from the $5p[3/2]_2$ to the $5p[3/2]_1$ levels of krypton as a function of pressure. The line through the points results from a least-square computer fit to the kinetic scheme presented in the text.

and $0.65 \times 10^{-12} \text{ cm}^3 \text{ sec}^{-1}$ (0.14 \AA^2) for excitation of $5p[3/2]_1$.

Unlike the other $\text{Kr}(5p)$ levels, emission from the $5p[5/2]_2$ state only could be observed indirectly. One transition (810.4 nm) from this state is overlapped by an argon line (scattering light from the discharge); and the second (877.7 nm) is detectable with our equipment only under the most favorable conditions. In order to obtain the pressure dependence of the $5p[5/2]_2$ state, the combined Ar and Kr intensities at 810.4 nm were compared with the intensity of another scattered argon line at 811.5 nm. Since the ratios of the scattered argon lines could be independently measured, the contribution to the 810.4 nm line when Kr was added to the reactor could be obtained. The total excitation of the $\text{Kr}(5p[5/2]_2)$ level was then obtained from the experimentally-determined intensity of the 810.4 nm line and the branching ratios of Murphy.⁸ The scatter in the experimental data, Fig. 3, for the pressure dependence of the $5p[5/2]_2$ level can be attributed to the difficulty of getting accurate values by difference from signals which are already quite small, and possibly to small changes in the ratio of the intensities of the scattered argon lines with pressure. Murphy's calculated values were used rather than the experimental numbers of Pery-Thorne and Chamberlain,⁹ because Murphy's calculations gave branching ratios for the 760.2–819.0 nm (3.08) and 769.5–829.8 nm (0.178) transitions that are in closer agreement with our values (3.26 ± 0.15 and 0.158 ± 0.012 , respectively) than are the experimental results (3.26 and 0.367) of Pery-Thorne and Chamberlain. In addition, Murphy's calculated lifetimes of the $5p[3/2]_2$ (25.4 nsec) and $5p[5/2]_3$ (28.5 nsec) states are in better agreement with the more recent determination by the Hanle effect¹⁰ (30.2 and 28.1 nsec, respectively) than are the results of Pery-Thorne and Chamberlain (47 and 59 nsec). The use of Pery-Thorne and Chamberlain's results would not, in any event, affect the conclusions based on the zero-pressure extrapolations.

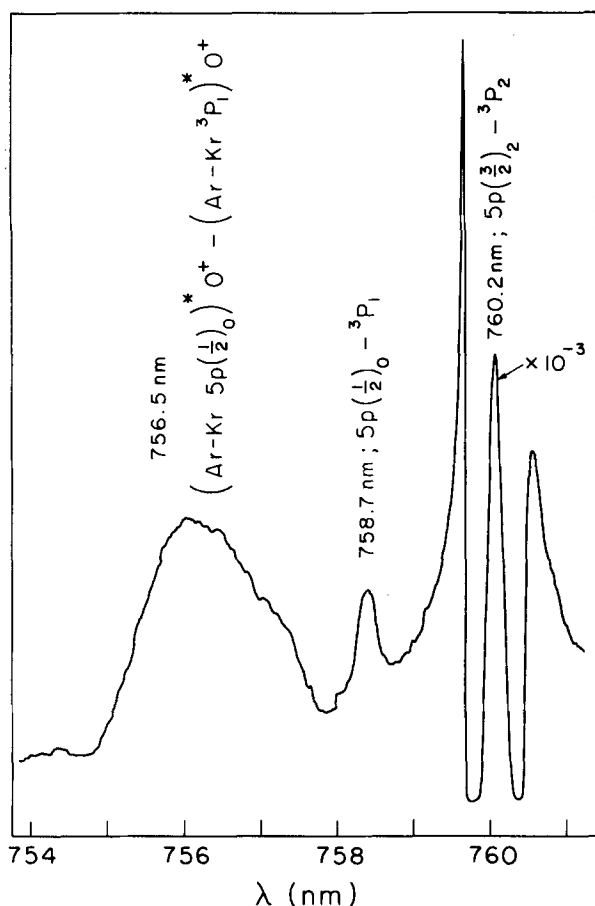


FIG. 5. Photoelectric scan of a portion of the krypton spectrum showing the ArKr excimer peaking at 756.5 nm, the 758.7 nm, $5p[1/2]_0-5s^3P_1$, atomic line [both of which are excited by $\text{Ar}^*(^3P_0)$], and the 760.2 nm, $5p[3/2]_2-5s^3P_2$, atomic line [excited by $\text{Ar}^*(^3P_2)$].

B. Excitation by $\text{Ar}^*(^3P_0)$

The $\text{Kr}(5p[1/2]_0)$ state is nearest in energy to $\text{Ar}^*(^3P_0)$ and, if populated, would emit at 758.7 nm. While searching for the 758.7 nm emission, a sideband feature to the blue of this line, as shown in Fig. 5, was found. The integrated intensities of the sideband, which peaks at 756.5 nm, and the atomic line were first order in krypton concentration. Initially, we were inclined to ascribe both the sideband and the atomic line to a structured excimer emission associated with the strong 760.2 nm line from $\text{Kr}(5p[3/2]_2)$. However, studies of the pressure dependence of the total integrated intensities of the sideband (hereafter called excimer) and of the atomic line, relative to the total emission intensity from all the $\text{Kr}(5p)$ levels (Fig. 6) and relative to each other (Fig. 7), suggested that both of these features were excited by $\text{Ar}^*(^3P_0)$. The general trend of the data in Fig. 6 shows that the excimer intensity declines with increasing pressure relative to the total $\text{Kr}(5p)$ emission intensity. If the excimer were associated with $\text{Kr}(5p[3/2]_2)$, an increase in this ratio with pressure would be expected. This decrease in excimer intensity relative to the total excitation [which nearly all arise from quenching of $\text{Ar}(^3P_2)$] can be explained if the excimer is

excited by $\text{Ar}^*(^3P_0)$, because $\text{Ar}(^3P_0)$ concentration will decrease relative to $\text{Ar}(^3P_2)$ concentration as the pressure increases (see below).

Figure 7 shows an increase in the 758.7 nm atomic-line intensity, relative to the excimer intensity, as pressure is increased. Since both the excimer and 758.7 nm atomic line are excited by $\text{Ar}^*(^3P_0)$, the excimer must be quenched in collisions with argon bath gas to account for the observed pressure dependence of Fig. 7. Figure 6 also shows that the 758.7 nm intensity increases with respect to the total $\text{Kr}(5p)$ emission intensity as the pressure increases, which is consistent with quenching of ArKr^* to $\text{Kr}(5p[1/2]_0)$. An interesting feature of the excimer is that the full-width at half-maximum changed from about 22 Å at the lowest pressure to about 15 Å at the higher pressure. This is evidence for vibrational relaxation in the upper state giving the excimer emission although, as mentioned later, the upper state of the excimer is not expected to be strongly bound.

The following steady-state kinetic analysis provides an explanation of these observations:

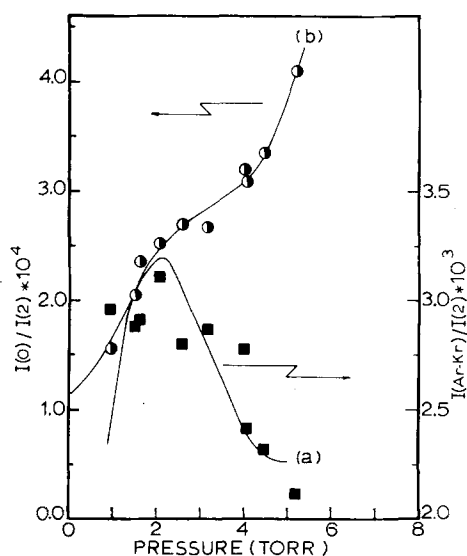
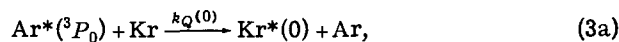
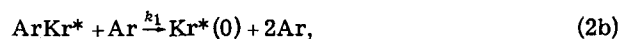
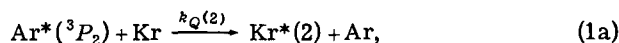


FIG. 6. The ratio of the intensity of the ArKr* excimer (a) and 758.7 nm atomic line (b) to the total intensity from all krypton levels as a function of pressure. The lines through the data are the results of least square computer fits of the data to the kinetic scheme outlined in the text.

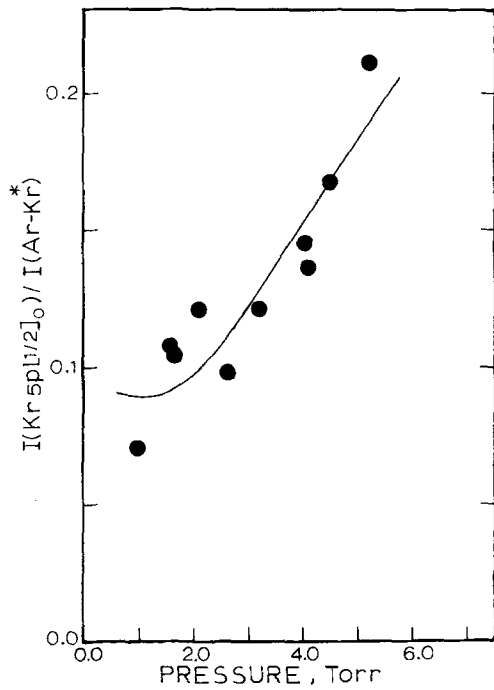
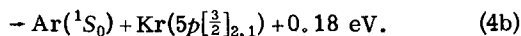
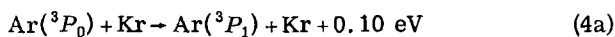


FIG. 7. The ratio of the integrated intensity of the 758.7 nm atomic (Kr) line to the integrated intensity of the excimer (KrAr). The line through the points is a computer fit to the kinetic scheme outlined in the text.

$\text{Kr}^*(2)$ represents all states excited by $\text{Ar}^*(^3P_2)$, and τ_1 is their composite lifetime; $k_Q(2) = 6.2 \times 10^{-12} \text{ cm}^3 \text{ molecule}^{-1} \cdot \text{sec}^{-1}$; $\text{Kr}^*(0)$ is $\text{Kr}(5p[1/2]_0)$, and $k_Q(0)$ is the excitation rate constant of $\text{Kr}^*(0)$ from $\text{Ar}^*(^3P_0)$. Steps (2a) and (3a) should not be construed as representing the total quenching for $\text{Ar}^*(^3P_0)$ because, as will be shown, other channels, such as (4), must be included in order to account for the total quenching rate constant for $\text{Ar}^*(^3P_0)$:



$$\frac{[\text{Ar}^*(^3P_0)]}{[\text{Ar}^*(^3P_2)]} = \frac{[\text{Ar}^*(^3P_0)]_0}{[\text{Ar}^*(^3P_2)]_0} \exp - \left(\{ [k_1(0) - k_1(2)] p^2 + [k_{II}(0) - k_{II}(2)] p^3 \} \frac{z}{f} \frac{\pi a_0^2}{RT} \right) \quad (9)$$

$$= \frac{[\text{Ar}^*(^3P_0)]_0}{[\text{Ar}^*(^3P_2)]_0} \exp - (Kp^2 + K'p^3). \quad (10)$$

Although the two-body quenching of $\text{Ar}(^3P_0)$ may give some 3P_2 , this will have a minor effect on the ratio because $[^3P_2]_0/[^3P_0]_0 \lesssim 5$. The use of (10) in Eqs. (5) and (7) allows the ratios to be fitted to changes in pressure for constant f .

A nonlinear least-squares computer program was used to extract the unknown terms $k_Q(m)$, $k_Q(0)$, $\tau_m k_1$, K , and K' by fitting the data of Figs. 6 and 7. It was not possible to obtain a reasonable fit to (5) and (7) when $\tau_m k_1$ was treated as a parameter to be determined

These processes were not directly observed and it is not necessary to include them in the following arguments, because any contribution to the $5p[3/2]_{2,1}$ emission intensities would be small and not strongly dependent on pressure. Equations (1)–(3) give steady-state expressions for the intensities which provide the following ratios:

$$\frac{I_{\text{ArKr}^*}}{I_2} = \frac{(k_Q(m)/k_Q(2))([\text{Ar}(^3P_0)]/[\text{Ar}(^3P_2)])[\text{Ar}]}{1 + \tau_m k_1 [\text{Ar}]}, \quad (5)$$

$$\frac{I_0}{I_{\text{KrAr}^*}} = \frac{k_Q(0)}{k_Q(m)[\text{Ar}]} + \frac{k_Q(0)\tau_m k_1}{k_Q(m)} + \tau_m k_1 [\text{Ar}],$$

$$\frac{I_0}{I_2} = \frac{k_Q(0)}{k_Q(2)} \frac{[\text{Ar}(^3P_0)]}{[\text{Ar}(^3P_2)]} + \frac{(\tau_m k_1 k_Q(m)/k_Q(2))([\text{Ar}(^3P_0)]/[\text{Ar}(^3P_2)])[\text{Ar}]^2}{1 + \tau_m k_1 [\text{Ar}]}. \quad (6)$$

Before proceeding with the analysis, the variation of $[\text{Ar}(^3P_0)]/[\text{Ar}(^3P_2)]$ with pressure must be considered.

In a flow reactor containing pure argon, a given metastable atom concentration will decay according to¹¹

$$[\text{Ar}^*] = [\text{Ar}^*]_0 \exp - \left\{ \left[\frac{D_0}{\Lambda^2} p^{-1} + k_{II} p + k_{III} p^2 \right] \frac{z}{v} \right\}, \quad (8)$$

where the subscript 0 refers to the initial concentration leaving the discharge; D_0/Λ^2 is the pressure-independent diffusion coefficient divided by the square of the characteristic diffusion length; k_I and k_{II} are the two- and three-body rate constants; and z/v is the distance from the metastable source to the observation region divided by the average bulk-flow velocity. The latter is equal to $fRT/P\pi a_0^2$, where f is the bulk-flow rate of gas, a_0 the flow-tube radius, and the other symbols have their usual meanings. The diffusion coefficients for the two metastables are the same, so that only differences in k_I and k_{II} are important.¹¹ Thus for a constant bulk-flow rate, $[\text{Ar}^*(^3P_0)]/[\text{Ar}^*(^3P_2)]$ will vary with pressure, as shown in (9) and (10).

by the computer program. Therefore, Eq. (6) was fitted to the data of Fig. 7 first to obtain the ratio $k_Q(0)/k_Q(m)$ and the quantity $\tau_m k_1 = (3.44 \pm 0.23) \times 10^{-2} \text{ torr}^{-1}$; the error limit is one standard deviation in the fit. Equations (5) and (7) next were fitted to the data of Fig. 6 with the explicit value of $\tau_m k_1$ just quoted. From Eq. (5) we obtained $K = (0.18 \pm 0.03) \text{ torr}^{-2}$, $K' = -(0.022 \pm 0.006) \text{ torr}^{-3}$, and

$$\frac{k_Q(m)}{k_Q(2)} \frac{[\text{Ar}^*(^3P_0)]_0}{[\text{Ar}^*(^3P_2)]_0} = (2.9 \pm 0.3) \times 10^{-3} \text{ torr}.$$

These values are not dependent on the value $\tau_m k_1$ as shown by repeating the calculations with $\tau_m k_1 = 0.03$ and 0.04 . The computer fit to Eq. (7) gave best-fit values $K = (0.195 \pm 0.03) \text{ torr}^{-2}$, $K' = -(0.026 \pm 0.004) \text{ torr}^{-3}$,

$$\frac{k_Q(0)}{k_Q(2)} \frac{[\text{Ar}^*(^3P_0)]_0}{[\text{Ar}^*(^3P_2)]_0} = (1.10 \pm 0.24) \times 10^{-4},$$

and

$$\frac{k_Q(m)}{k_Q(2)} \frac{[\text{Ar}^*(^3P_0)]_0}{[\text{Ar}^*(^3P_2)]_0} = (2.5 \pm 0.5) \times 10^{-3} \text{ torr}^{-1}.$$

In this case only the last quantity showed any variation with the choice of $\tau_m k_1$, but this variation was less than the standard deviation. Using the values obtained above, $k_Q(2)$ and the ratio $[\text{Ar}^*(^3P_0)]_0/[\text{Ar}^*(^3P_2)]_0 = 0.20$ (as determined from zero-pressure extrapolations in former absorption studies^{11b,2b}), $k_Q(m) = 2.5 \times 10^{-30} \text{ cm}^6 \text{ molecule}^{-2} \cdot \text{sec}^{-1}$ and $k_Q(0) = 3.4 \times 10^{-15} \text{ cm}^3 \text{ molecule}^{-1} \cdot \text{sec}^{-1}$. The ratio $k_Q(0)/k_Q(m)$ evaluated from the results of the fits to Eqs. (5) and (7) is 0.041 torr , which is comparable, within the error of the fits, to the value of 0.053 obtained from the fit to Eq. 6. These rate constant values are summarized in Table I.

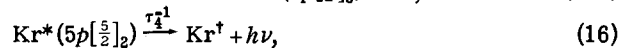
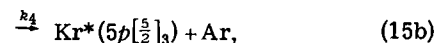
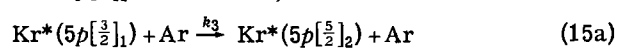
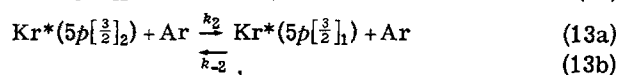
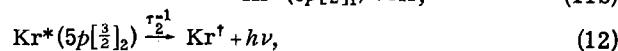
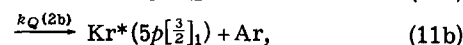
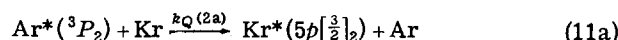
As a check upon this analysis, the values of K and K' can be examined using accepted values of rate constants¹¹ and properties of our apparatus $k_1(0) = 5.4 \times 10^{-15}$ and $k_1(2) = 1.3 \times 10^{-15} \text{ cm}^3 \text{ molecule}^{-1} \cdot \text{sec}^{-1}$; $k_{II}(0) = 1.14 \times 10^{-32}$ and $k_{II}(2) = 1.7 \times 10^{-32} \text{ cm}^6 \text{ molecule}^{-2} \cdot \text{sec}^{-1}$, $z = 7.5 \text{ cm}$, $a_0 = 0.5 \text{ cm}$, and $f = 2.4 \times 10^{-4} \text{ mole sec}^{-1}$. These numbers give $K = 0.18 \text{ torr}^{-2}$, in agreement with the computer-fit value of 0.19 torr^{-2} , and $K' = -8.0 \times 10^{-3} \text{ torr}^{-3}$, a factor of 3 smaller than the computer-fit value of $-2.4 \times 10^{-2} \text{ torr}^{-3}$. This discrepancy is not distressing, because the three-body de-excitation rates of metastable argon are not well established and published values for $k_{II}(2)$ vary between 0.62 and $2.4 \times 10^{-32} \text{ cm}^6 \text{ molecule}^{-2} \cdot \text{sec}^{-1}$,¹¹ while $k_{II}(0)$ has been determined only once.^{11a} Furthermore, the computer fitted values have at least a factor of 2 uncertainty associated with them because of the complexity of the flow pattern from the discharge to mixing zone.

The preceding analysis fits the data of Figs. 6 and 7

remarkable well. However, the scheme was proposed to explain existing data and diagnostic experiments confirming and testing the proposed steps have not been done. Therefore the qualitative features are probably more important than the quantitative fit. Assuming that the rate constants $k_Q(0)$ and $k_Q(m)$ are roughly correct, the total apparent bimolecular rate constant for product formation at 1 torr pressure is $3.4 \times 10^{-15} + 8.2 \times 10^{-14} = 8.5 \times 10^{-14} \text{ cm}^3 \text{ molecule}^{-1} \cdot \text{sec}^{-1}$, which is a factor of 27 lower than the total quenching rate constant. This is the basis for the claim that a large fraction of the quenching must proceed via processes such as (4).

C. Collisional cascade within the Kr(5p) levels

Kinetic analysis of the pressure dependences of the populations of the various Kr(5p) levels was done according to the following scheme:



Steady state analysis leads to two very simple relationships;

$$\frac{I5p[\frac{3}{2}]_2}{I5p[\frac{3}{2}]_1} = \tau_3 k_3 [\text{Ar}] \text{ and } \frac{I5p[\frac{3}{2}]_3}{I5p[\frac{3}{2}]_1} = \tau_3 k_4 [\text{Ar}].$$

Linear least-square fit to the data of Fig. 3 gave $k_3 = 2.5 \pm 0.25 \times 10^{-11} \text{ cm}^3 \text{ molecule}^{-1} \cdot \text{sec}^{-1}$ and $k_4 = 4.2 \pm 0.5 \times 10^{-11} \text{ cm}^3 \text{ molecule}^{-1} \cdot \text{sec}^{-1}$ for a value of $\tau_3 = 29.9 \text{ nsec}$.⁸

Additional relationships are

$$\frac{I5p[\frac{3}{2}]_2}{I_T} = \left(\frac{I5p[\frac{3}{2}]_2}{I_T} \right)_0 \frac{1 + \{ \tau_3 k_{-2} [1 + k_Q(2b)/k_Q(2a)] + \tau_3 (k_3 + k_4) \} [\text{Ar}]}{1 + A [\text{Ar}] + B [\text{Ar}]^2}, \quad (18)$$

$$\frac{I5p[\frac{3}{2}]_1}{I_T} = \left(\frac{I5p[\frac{3}{2}]_1}{I_T} \right)_0 \frac{1 + \{ \tau_2 k_2 [1 + k_Q(2a)/k_Q(2b)] \} [\text{Ar}]}{1 + A [\text{Ar}] + B [\text{Ar}]^2}, \quad (19)$$

where $A = \tau_2 k_2 + \tau_3 (k_{-2} + k_3 + k_4)$, $B = \tau_2 \tau_3 k_2 (k_3 + k_4)$, and I_T is equal to the total krypton emission intensity. The 0 subscript denotes the zero-pressure intensity ratio. Equations (18) and (19) are too complex and the data are too scattered to obtain rate constants by fitting them to Fig. 2; however, a computer fit of the data of Fig. 4 to the $I5p[\frac{3}{2}]_2/I5p[\frac{3}{2}]_1$ ratio can be used to obtain k_2 , k_{-2} , and $k_3 + k_4$:

$$\frac{I5p[\frac{3}{2}]_2}{I5p[\frac{3}{2}]_1} = \frac{k_Q(2a)}{k_Q(2b)} \frac{1 + \{ \tau_3 (k_3 + k_4) + \tau_3 k_{-2} [1 + k_Q(2b)/k_Q(2a)] \} [\text{Ar}]}{1 + \tau_2 k_2 [1 + k_Q(2a)/k_Q(2b)] [\text{Ar}]} \quad (20)$$

TABLE I. Rate constants determined from analysis of emission data from $\text{Ar}((^3P_{0,2}) + \text{Kr})$.

Process	Rate constant
$\text{Ar}*(^3P_2) + \text{Kr} \rightarrow \text{products}$	$6.2 \times 10^{-12} \text{ }^{\text{a,b}}$
$\rightarrow \text{Kr}*(5p[{}^3_2]_2)$	$5.5_5 \times 10^{-12} \text{ }^{\text{b}}$
$\rightarrow \text{Kr}*(5p[{}^3_2]_1)$	$0.65 \times 10^{-12} \text{ }^{\text{b}}$
$\text{Ar}*(^3P_0) + \text{Kr} \rightarrow \text{products}$	$2.3 \times 10^{-12} \text{ }^{\text{a,b}}$
$\text{Ar}*(^3P_0) + \text{Kr} + \text{Ar} \rightarrow \text{ArKr}^* + \text{Ar}$	$2.5 \times 10^{-30} \text{ }^{\text{c}}$
$\text{Ar}*(^3P_0) + \text{Kr} \rightarrow \text{Kr}*(5p[{}^1_2]_0) + \text{Ar}$	$3.4 \times 10^{-15} \text{ }^{\text{b}}$
$\text{ArKr}^* + \text{Ar} \rightarrow \text{Kr}*(5p[{}^1_2]_0) + 2 \text{ Ar}$	$1.0 \times 10^{-18} \text{ }^{\text{d}}$

^aReference 2b.^bUnits $\text{cm}^3 \text{ molecule}^{-1} \cdot \text{sec}^{-1}$.^cUnits $\text{cm}^6 \text{ molecule}^{-2} \cdot \text{sec}^{-1}$.^dProduct of the quenching rate constant and radiative lifetime; units $\text{cm}^3 \text{ molecule}^{-1}$.

Equation (20) is of the form $R = A(1) \{ [1 + A(2)p] / [1 + A(3)p] \}$ and the computer fit of the data to this equation gave $A(1) = 8.6 \pm 4\%$, $A(2) = 0.078 \text{ torr}^{-1} \pm 100\%$, and $A(3) = 0.13 \text{ torr}^{-1} \pm 100\%$. The $A(3)$ value gives $k_2 = 1.4 \times 10^{-11} \text{ cm}^3 \text{ molecule}^{-1} \cdot \text{sec}^{-1}$ when combined with $\tau_2 = 30.2 \text{ nsec}$ ¹⁰ and $A(1)$ which is just $k_Q(2a)/k_Q(2b)$ and is determined from the intercept. The principle of detailed balance gives $k_{-2} = 0.280 k_2$ so that we may determine $k_3 + k_4 = 7.5 \times 10^{-11} \text{ cm}^3 \text{ molecule}^{-1} \cdot \text{sec}^{-1}$ from $A(2)$ when $\tau_3 = 29.9 \text{ nsec}$ ⁸ is used along with the other parameters determined above. This $k_3 + k_4$ value is equal to the sum of the values determined separately. These rate constant values are listed in Table II.

We tried a more complete treatment which included direct quenching of the $5p[{}^3_2]_2$ level to the $5p[{}^3_2]_{2,3}$ levels and collisional transfer between the two lower levels, but the results were essentially the same as presented above, i. e., no direct cascade from $5p[{}^3_2]_2$ ($k < 10^{-12} \text{ cm}^3 \text{ molecule}^{-1} \cdot \text{sec}^{-1}$) to the $5p[{}^3_2]_{2,3}$ levels and no discernible transfer between $5p[{}^3_2]_2$ and $5p[{}^3_2]_3$ levels ($k \leq 6 \times 10^{-12} \text{ cm}^3 \text{ molecule}^{-1} \cdot \text{sec}^{-1}$). Since the $5p[{}^1_2]_1$ level could not be observed readily, collisional cascade to the level was not studied.

D. Absorption of Kr resonance radiation at 123.6 nm

In order to examine the hypothesis that $\text{Ar}(^3P_{0,2})$ excites only the $\text{Kr}(5p)$ levels, vacuum ultraviolet studies were done to test for direct formation of $\text{Kr}(5s, ^1P_1)$ and $\text{Kr}(5s, ^3P_1)$. No emission was observed from the $5s^1P_1$ resonance level which emits to the ground Kr level at 116.5 nm. Radiative cascade from the $5p$ levels to the 1P_1 state is not favored because the transition probability⁸ to this state is only about 0.25% of the transition probability to either $\text{Kr}(^3P_1)$ or $\text{Kr}(^3P_2)$. Minor direct excitation of the 1P_1 state cannot be completely eliminated, since the 116.5 nm emission is in an extremely unfavorable region of the spectrum for our optical system.

The 123.6 nm line from the $\text{Kr}(^3P_1 - ^1S_0)$ transition was observed. Direct excitation can be tested experimentally since the energy defect for formation from

$\text{Ar}(^3P_2)$ is 1.5 eV and any direct excitation of $5s^3P_1$ would give a strongly broadened emission line. For an equivalent Doppler emission line, at an effective temperature T_s , and for a Doppler absorber at T_a (300 °K), $\alpha = (T_s/T_a)^{1/2} = 7.65$.¹² On the other hand, excitation by radiative cascade from the $5p[{}^3_2]_{1,2}$ levels of Kr would give a nearly-thermal Doppler emission profile ($\alpha = 1$), since the $\text{Kr}(5p[{}^3_2]_{1,2})$ levels have nearly the same energy as $\text{Ar}(^3P_2)$. Because the radiative lifetime¹³ of the 3P_1 level is very short ($\sim 4 \text{ nsec}$), thermalization of the emission line by momentum transfer with argon bath gas atoms does not complicate these conclusions. Excitation transfer, which is an alternative mechanism for thermalization, is also ruled out because of the low concentration of ground state Kr atoms.

The f value for the 123.6 nm transition has been studied numerous times; Geiger,¹³ Turner,¹⁴ and Stacey¹⁵ all give values of 0.17, while Vaughan¹⁶ (as modified by the theoretical work of Berman and Lamb)¹⁷ and Griffin and Hutcherson obtained values of 0.19.¹⁸ We reanalyzed the data of Griffin and Hutcherson to include their studies on the resonance broadening of the 123.6 nm line¹⁹ (using the work of Berman and Lamb to provide the model) and find that an f value of 0.17 gives a better fit to all of their data. Other values which have been obtained such as the 0.16 of Wilkinson²⁰ and the 0.21 of Chaschina and Shreider²¹ are suspect, since these works contain mistakes or uncertainties in experimental parameters. Thus, $f = 0.17$ was used for computation of α for the $\text{Kr}(^3P_1)$ emission in our metastable studies.

The equivalent Doppler width of the 123.6 nm line of Kr produced by $\text{Ar}(^3P_{0,2}) + \text{Kr}$ was determined from measurements of α using an absorption technique. Measurements of integrated line absorption were made as a function of known concentrations of Kr atoms in a flow cell placed between the $\text{Kr}(^3P_1)$ source and the detector. The value of $f = 0.17$ for the 123.6 nm transition was used in the computations¹² to give the corresponding value of α . [Corrections ($\leq 20\%$) for self-reversal of the Kr 123.6 nm radiation were made using the two-layer model with the second, self-reversing layer at 300 °K. The path length for this correction was taken to be the radius of the metastable flow tube, in order to calculate the corresponding optical depth in the reversing layer, $k_0 m$.] Figure 8 shows the results of the absorption experiments in terms of plots of absorber optical depth, $k_0 l$, against $[\text{Kr}]$, derived from

TABLE II. Collisional cascade rate constants within the Kr ($5p$) levels.

Process	Rate constant ($\text{cm}^3 \text{ molecule}^{-1} \cdot \text{sec}^{-1}$)
$\text{Kr}*(5p[{}^3_2]_2) + \text{Ar} \xrightarrow{k_2} \text{Kr}*(5p[{}^3_2]_1) + \text{Ar}$	1.4×10^{-11}
$\xrightarrow{k_{-2}}$	0.39×10^{-11}
$\text{Kr}*(5p[{}^3_2]_1) + \text{Ar} \xrightarrow{k_3} \text{Kr}*(5p[{}^3_2]_2)$	2.5×10^{-11}
$\xrightarrow{k_4} \text{Kr}*(5p[{}^3_2]_3)$	4.2×10^{-11}

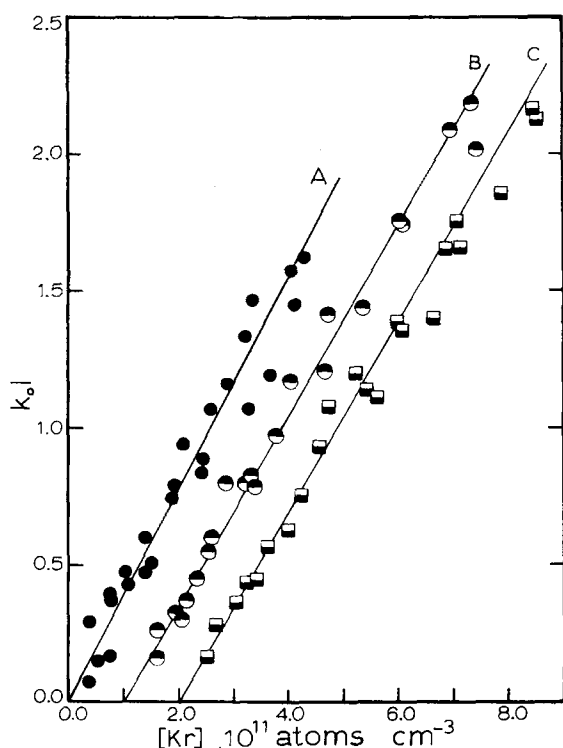


FIG. 8. The absorption of the Kr 126 nm line vs concentration of Kr in the absorption chamber for three different concentrations (A—2.3, B—4.9, and C— 13.2×10^{11} atoms/cm³) of Kr in the emission source, which corresponds to $k_0 m = 0.5$ (A), 1.0 (B), and 2.5 (C). The points for B and C have been moved to the right by one and two concentration units, respectively, for convenience of presentation. The lines are least square fits to the points.

the raw absorption data using standard programs.¹² The values for α derived from the three experiments were 1.03 ± 0.25 , 1.13 ± 0.15 , and 1.10 ± 0.11 , which within experimental error correspond well with the value $\alpha = 100$. Realistic limits of error for this technique are $\alpha = 1.00 \pm 0.25$. Therefore, no significant Doppler broadening above that for 300 °K was found in the Kr(³P₁) emitter. These absorption studies hence provide confirmation that the major primary product channels for Ar(³P_{0,2}) are Kr($5p[\frac{3}{2}]_{2,1}$) rather than Kr($5s, {}^3P_1$).

IV. DISCUSSION

A. Quenching mechanism for Ar(³P₂) + Kr

The only states of krypton excited by Ar*(³P₂) are the $5p[\frac{3}{2}]_2$ and $5p[\frac{3}{2}]_1$ levels with exoergicities of 0.0025 and 0.002 eV, respectively. The mechanism for the quenching process leading to these excitations clearly cannot be of the resonance dipole-dipole type²² since the optical selection rules of this mechanism do not permit $4p \rightarrow 5p$ excitation. Neither is the mechanism likely to be a curve crossing involving an ionic intermediate³ since rare-gas negative ions are unbonded species. By process of elimination, a direct crossing of entrance and exit channels or perhaps a curve merging or direct coupling of entrance and exit channels along the entire range of internuclear distances covered by the potential curves appear to be the likely quenching

mechanism. The latter mechanism, recently applied²³ with great success to the charge transfer reaction in the Li-Na⁺ system, cannot be tested without resorting to involved calculations. We therefore will confine the remainder of our discussion to the simple curve crossing mechanism. The input channel consists of molecular configurations of 0⁻, 1, and 2; the $5p[\frac{3}{2}]_2$ exit channel is 0⁺, 1, and 2 and the $5p[\frac{3}{2}]_1$ exit channel is 0⁻ and 1. Thus symmetry does not impose any significant restrictions or favor one exit channel over the other.

Figure 9 shows the potential curves which will serve as the basis for our discussion. The entrance channel was derived from the differential scattering measurements of Winicur and Fraites.⁶ Nenner²⁴ also measured the Ar(³P₂) + Kr potential in a molecular beam study of the variation of the total cross section as a function of relative velocity. The two studies agree on the position of the potential minimum, but Nenner's well depth is only half that of Winicur and Fraites.^{6,25} The splitting of the entrance channel into the 0⁻, 1, and 2 components presumably will occur at shorter r , but this should not be important for quenching because the exit channels are repulsive and cross $V(\text{Ar}^* + \text{Kr})$ at $r > r_m$.

The shapes of the two exit channels were assumed to be the same, but displaced by the difference in the asymptotic energy limits, this cannot be completely correct since the $5p[\frac{3}{2}]_2$ state is quenched to the $5p[\frac{3}{2}]_1$ state. Vaughan and Smith²⁶ obtained the difference potential (using a Lennard-Jones model) between Kr*($5p$)—

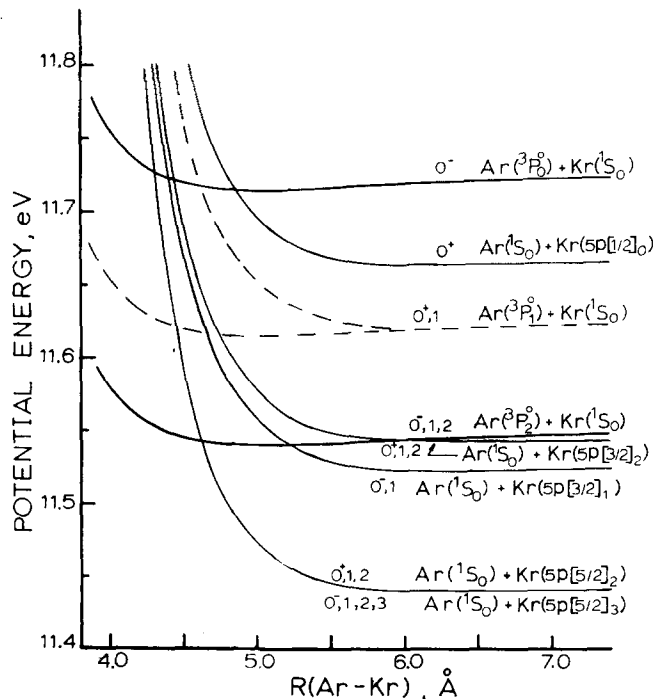


FIG. 9. Potential energy curves for Ar*($4s$) + Kr [drawn from the Ar(³P₂) + Kr potential, Ref. 6] and Kr($5p$) + Ar (see text for potential). The potentials for various Ar($4s$) or the Kr($5p$) states and Ω components (indicated by the numbers) presumably differ in detail, but additional information is required before these differences can be known. The splitting into the different Ω components is more important at short range. The dotted curves shown for Ar(³P₁^o) are two examples, namely the Ar* (metastable) + Kr and the Kr*($5p$) + Ar curves.

Ar and Kr*(5s)-Ar by measuring the Lorentz broadening and shift of several krypton lines at 295° and 80° K. Although their data are not particularly sensitive to the repulsive part of the potential, within the limits of the Lennard-Jones model, repulsive constants consistent to within about a factor of 2 can be derived from their measurements. We thus have for the difference potential²⁷ $\Delta C_6 = 4.3 \times 10^{-58}$ erg · cm⁶ and $\Delta C_{12} = 2.0 \times 10^{-101}$ erg · cm¹². Combining these results with the potential for Kr*(5s) + Ar gives the potential for Kr*(5p) with Ar. The Slater-Kirkwood approximation was used to determine C_6 for Kr*(5s)-Ar, and the r_m value was taken from the elastic scattering measurements of Rb + Ar.²⁸ Since the experimental polarizability of Kr(³P₂) is available,²⁹ the Slater-Kirkwood C_6 should be a reasonably good estimate. For example, the Slater-Kirkwood C_6 for Ar*(³P₂)-Kr lies between the experimental values of Nenner and of Winicur and Fraites. The r_m values for the metastable rare gas are known to closely resemble the values for the corresponding alkali rare gas.²⁵ The end result for Kr*(5s) + Ar potential constants are $C_6 = 2.65 \times 10^{-58}$ erg · cm⁶ and $C_{12} = 2.51 \times 10^{-102}$ erg · cm¹², which give $C_6 = 6.99 \times 10^{-58}$ erg · cm⁶ and $C_{12} = 2.25 \times 10^{-101}$ erg · cm¹² for Kr*(5p)-Ar.

The simple Landau-Zener theory³⁰ can be used to relate the cross section for the excitation process to the probability of crossing from one potential curve to the other:

$$P_x = 2 \exp(-\eta_x)(1 - \exp(-\eta_x)), \quad (21)$$

$$\eta_x = \frac{2\pi}{\hbar v_x} * \frac{V_{12}^2(R_x)}{d/dR |V_1 - V_2|_{R_x}}. \quad (22)$$

The interaction matrix element V_{12} is evaluated at the crossing distance R_x ; $d/dR |V_1 - V_2|_{R_x}$ is the absolute value of the difference in potential gradients of the diabatic curves at R_x ; v_x is the relative velocity of the colliding particles at R_x ; and the other symbols have their usual meanings. For small P_x , the rate constant for a thermal process can be expressed³⁰ as

$$k = \langle v \rangle \sigma = \langle v \rangle \pi R_x^2 \langle P_x \rangle, \quad (23)$$

where $\langle v \rangle$ and $\langle P_x \rangle$ are the Boltzmann averaged velocity and transition probability, respectively. If the crossing occurs on the repulsive wall of the input channel, a Boltzmann factor is appended to Eq. (23), but according to Fig. 9 this does not apply here. Using the crossing points R_x as determined from the potential curves in Fig. 9 and the rate constants from this work, $\langle P_x \rangle = 5.2 \times 10^{-3}$ for the $5p[\frac{3}{2}]_2$ crossing at 5.96 Å and 9.2×10^{-4} for the $5p[\frac{3}{2}]_1$ crossing at 5.21 Å.

There are two limiting cases for small $\langle P_x \rangle$ in the Landau-Zener theory. Either the curves in the crossing region are almost pure diabatic curves (as shown in Fig. 9) so that the adiabatic coupling is small (case 1), or else the adiabatic coupling is strong so that the curves should be redrawn to conform to adiabatic changes in potential energy in the region of the crossing (case 2). In case 1 $\exp(-\eta_x) \approx 1$, so that the limiting probability is $\approx [1 - \exp(-\eta_x)] \approx \eta_x$. For case 2, $\exp(-\eta_x) \ll 1$ and $P_x \approx \exp(-\eta_x)$. For case 1, with $V_{12}(R_{x1}) \approx V_{12}(R_{x2})$ the differences in $\langle P_x \rangle$ primarily will be governed by the

potential-gradient differences:

$$\frac{P_{x1}[5p[\frac{3}{2}]_2]}{P_{x2}[5p[\frac{3}{2}]_1]} \approx \frac{d/dR |V_1 - V_{5p(3/2)_1}|_{R_{x2}}}{d/dR |V_1 - V_{5p(3/2)_2}|_{R_{x1}}}. \quad (24)$$

The potential-gradient differences can be obtained by differentiation of the potentials in Fig. 9 (at the appropriate crossing points); the ratio is 6.0, which compares favorably with the probability ratio of 6.3. The good agreement between theory and experiment is somewhat fortuitous, as Kr*(5p)-Ar potential curves are not well known and the effect of the different couplings and Ω values have not been included in $\langle P_x \rangle$.

In order to explain the difference in probabilities for the $5p[\frac{3}{2}]_2$ and $5p[\frac{3}{2}]_1$ exit channels according to case 2, the interaction potential at the crossing point for $5p[\frac{3}{2}]_1$ must be significantly larger than for crossing of the $5p[\frac{3}{2}]_2$ curve. The interaction V_{12} would have to be on the order of 1 eV at R_x for $5p[\frac{3}{2}]_1$, which is unrealistically large. Thus the explanation based upon case 1 considerations is favored.

In a molecular beam study, Winicur and Fraites⁶ also concluded that Kr(5s ³P_{0,2}) was formed by radiative cascade rather than directly by the Ar(³P₂) + Kr reaction. The cross section for energy exchange [as detected by Kr(³P_{2,0}) formation] appeared to increase with kinetic energy up to ~75 meV and then to subsequently decline with higher energy.

B. Quenching mechanisms for Ar*(³P₀) and Kr

Interaction of Ar(³P₀) and Kr excites the $5p[\frac{1}{2}]_0$ level of Kr in a slow two-body step and gives an ArKr* excimer in a relatively fast three-body step. However, the main process must be transfer to Ar*(³P₁) or formation of Kr($5p[\frac{3}{2}]_1$) or Kr($5p[\frac{3}{2}]_2$). The curve-crossing mechanism can explain the much smaller excitation of Kr($5p[\frac{1}{2}]_0$) relative to excitation of the close lying Kr5p states by Ar*(³P₂), because the symmetry of the Ar*(³P₀) + Kr potential is 0⁻ while the exit channel is an 0⁺ state (see Fig. 9). Thus the mixing of the two states cannot be effected.

The observed excimer emission must be from the Kr($5p[\frac{1}{2}]_0$ -Ar)₀₊ state to the Kr(³P₁-Ar)₀₊ state. The three-body collision destroys symmetry restrictions so the efficient three-body formation rate is not surprising. Tanaka *et al.*³² observed both of these 0⁺ states in vacuum uv absorption experiments. Since this emission appears only slightly to the blue of the Kr($5p[\frac{1}{2}]_0$ -³P₁) line, the lower state must have the stronger binding energy, which is in agreement with the results of Tanaka *et al.*

Since the observed two- and three-body steps are only a small fraction of the total quenching rate constant, the remainder of the quenching must give other states and Ar(³P₁), Kr($5p[\frac{3}{2}]_1$), or Kr($5p[\frac{3}{2}]_2$) are the most likely possibilities. As shown in Fig. 9 neither the Ar(³P₁) + Kr or Ar + Kr($5p[\frac{3}{2}]_2$) have an 0⁻ state. However, for nonzero impact parameters, e.g., an Ar(³P₀)-Kr molecule with $J' > 0$, transfer to the $\Omega = 1$ and 2 dis-

sociative $\text{Ar}(^3P_1)\text{-Kr}$ or $\text{Ar-Kr}(5p[\frac{3}{2}]_2)$ states is allowed according to rules for predissociation. If the potential curves for $\text{Ar}(^3P_0)+\text{Kr}$ and $\text{Ar}(^3P_1)+\text{Kr}$ are identical, there obviously can be no crossing. However, the $\Omega=1$ curve probably is more repulsive than the 0^- curve, and even a minor change in the repulsion parameter will give a crossing. For example, as shown in Fig. 9, if the $\text{Kr}(5p)+\text{Ar}$ potential is used to represent the $\text{Ar}(^3P_1)\text{-Kr}$ curve (which is an overestimate of the repulsion), the crossing occurs but the intersection is too abrupt to be a good exit channel. The parameters chosen for the $\text{Ar}+\text{Kr}^*(5p)$ curves do lead to favorable intersections of $\text{Ar}+\text{Kr}(5p[\frac{3}{2}]_{1,2})$ with the $\text{Ar}(^3P_0)+\text{Kr}$ potential; however, this may be fortuitous. In general, we favor $\text{Kr}(5p[\frac{3}{2}]_2)$ and $\text{Kr}(5p[\frac{3}{2}]_1)$ as exit channels because the quenching rate constant of $\text{Ar}(^3P_0)$ by Kr is ~ 3 orders of magnitude greater than the two-body rate by Ar,^{11b} which suggests that the $\text{Ar}(^3P_1)$ channel is not the important one.

C. Mechanism for collisional cascade of $\text{Kr}(5p)$ levels

The mechanism for collisional cascade within the $\text{Kr}(5p)$ levels, specifically the transfer between the $5p[\frac{3}{2}]_2$ and $5p[\frac{3}{2}]_1$ and between the $5p[\frac{3}{2}]_1$ and $5p[\frac{5}{2}]_{2,3}$ levels, must involve a curve crossing. Since the valence electrons of the excited Kr atoms correlating with these molecular states are $p-\pi$ electrons, the various Ω components of the molecular states may separate at fairly large internuclear distance. Thus a crossing between the 1 and 0^+ states in the $5p[\frac{3}{2}]_1-5p[\frac{3}{2}]_2$ interaction and between the 1 curves of the $5p[\frac{3}{2}]_{2,3}$ states with the 0^- curve for the $5p[\frac{3}{2}]_1$ state could occur. The $5p[\frac{5}{2}]_2$ state may give attractive curves³¹ so that this state could be populated solely from interaction with the $5p[\frac{5}{2}]_3$ state. Indeed, the rates of formation of these two states are roughly in proportion to the statistically expected distribution. More complete knowledge about the potentials will be necessary before a more detailed treatment of these processes can be attempted.

D. The $\text{Ar}(^3P_2)+\text{Kr}$ reaction as a reference for measurements of other $\text{Ar}(^3P_2)$ excitation rate constants and as an absolute emission source in the vacuum u.v.

Since quenching of $\text{Ar}^*(^3P_2)$ by Kr results only in formation of $\text{Kr}(5p[\frac{3}{2}]_{1,2})$, the $\text{Ar}(^3P_2)+\text{Kr}$ reaction is an excellent reference for obtaining quenching rates for excitation of other atoms and molecules by argon metastables. Furthermore, the simultaneous determination of $[\text{Ar}(^3P_2)]$, $[\text{Kr}]$, and the Kr^* emission intensity permits the calibration of an apparatus with respect to absolute emission intensity. The measurement of $[\text{Ar}(^3P_2)]$ is relatively straightforward by absorption spectroscopy,^{2b} since the oscillator strength for several $4s-4p$ transitions are known.

Before accepting these claims, which are based upon quenching of $\text{Ar}(^3P_2)$ by Kr via only energy transfer to the $\text{Kr}(5p)$ levels, quenching by transfer to $\text{Ar}(^3P_1)$ and by collision-induced radiation should be considered because these are observed processes for decay of the heavy metastable states in the parent rare gas. The

rate constant for the sum of these two processes^{11,32-34} are $\sim 10^{-15}$ cm^3 molecule⁻¹ sec⁻¹ for the 3P_2 metastable states of Ar, Kr, and Xe. The $\text{Xe}(^3P_2)+\text{Ar}$ mixed rare-gas system shows similar behavior,³⁵ and destruction of $\text{Ar}(^3P_2)$ by Kr should, therefore, contain only an insignificantly small contribution from these two processes. Thus, we are confident in attributing the quenching of $\text{Ar}^*(^3P_2)$ to formation of only $\text{Kr}(5p[\frac{3}{2}]_{2,1})$ products.

Since the quenching rate constant of $\text{Ar}(^3P_2)$ by Kr and the excitation rate constants for $\text{Kr}(5p[\frac{3}{2}]_{1,2})$ are the same, this system can be used to obtain absolute-excitation rates of other emission processes excited by metastable argon. This can be done easily in the infrared to near uv region by direct comparison of the emission intensities from Kr^* to that from an additive for known concentration of Kr and additive. The total pressure should be sufficiently low that collisional cascade within the $\text{Kr}(5p)$ levels or quenching of the additive states are avoided. Emission from $\text{Kr}(5p[\frac{3}{2}]_2)$ is the best reference; radiative branching favors $\text{Kr}(5s^3P_2)$ over $\text{Kr}(5s^3P_1)$ by a factor of 3.3. The radiative cascade to the $\text{Kr}(5s^3P_1)$ permits the resonance line at 123.6 nm to be used as a reference in the vacuum ultraviolet. Appropriate allowance must be made for branching, because only 0.301 ± 0.006 of the initial $\text{Kr}(5p[\frac{3}{2}]_{2,1})$ excitation cascades to the 3P_1 level. Also, some caution must be exercised because even for low krypton concentration the 123.6 nm line can be self-absorbed. This effect will reduce the observed photon yield from krypton which will, in turn, lead to an overestimate of the excitation rate constant from the additive. Our absorption experiments show that small corrections for self-absorption of the 123.6 nm emission can be made as long as the krypton concentration is sufficiently low that the optical depth between the interaction region and the monochromator is less than about $2.5 (\sim 1.3 \times 10^{12}$ atoms \cdot cm^3 in a 30 mm i.d. tube). For these conditions the two-layer model can then be used to estimate the initial krypton resonance emission intensity.

V. SUMMARY AND CONCLUSIONS

The quenching of $\text{Ar}(^3P_2)$ by krypton results only in the excitation of $\text{Kr}(5p[\frac{3}{2}]_2)$ and $(5p[\frac{3}{2}]_1)$. Studies of the pressure dependence of the $5p$ krypton-level populations and the linewidth of the $\text{Kr}(5s, ^3P_1-^1S_0)$ resonance line at 123.6 nm show that all other observed excitations result from either collisional or radiative cascade. Approximate rate constants were obtained for collisional cascade within the $5p$ levels of krypton.

The excitation of krypton by $\text{Ar}^*(^3P_2)$ can be explained quite adequately by a simple Landau-Zener curve crossing model. Thus with the $\text{Ar}(^3P_2)+\text{Kr}$ example there are examples of quenching reactions which occur by four major types of mechanisms: "golden rule type,"^{2b} ionic-intermediate curve crossing,³ simple crossing of entrance and exit channels, and chemical reaction.^{36,4}

The quenching of $\text{Ar}^*(^3P_0)$ by krypton has a reduced rate constant, relative to $\text{Ar}(^3P_2)$, which can be rational-

ized in the simple curve crossing model by symmetry restrictions which restrict the coupling of the entrance and exit channels. Quenching of $\text{Ar}(^6P_0)$ was accompanied by an excimer emission which is associated with the $\text{Kr}(5p[\frac{1}{2}]_0)$ level.

ACKNOWLEDGMENTS

The support provided by the U.S. Army Research Office-Durham (DAHCO4-75-G0018) at Kansas State University and by the Science Research Council at Queen Mary College are gratefully acknowledged. We thank Professor Winicur for sending us a preprint of Ref. 6. One of us (L.G.P.) also wishes to acknowledge discussions with Dr. P. Siska of the University of Pittsburgh.

- ¹(a) D. H. Stedman and D. W. Setser, *Prog. React. Kinet.* **6**, 193 (1971); (b) G. W. Taylor, D. W. Setser, and J. Coxon, *J. Mol. Spectrosc.* **44**, 108 (1972); (c) G. W. Taylor, *J. Phys. Chem.* **77**, 124 (1973); (d) J. A. Coxon, D. W. Setser, and W. H. Duerwer, *J. Chem. Phys.* **58**, 2244 (1973); (e) W. C. Richardson and D. W. Setser, *J. Chem. Phys.* **58**, 1809 (1973).
- ²(a) L. G. Piper, W. C. Richardson, G. W. Taylor, and D. W. Setser, *Discuss. Faraday Soc.* **53**, 100 (1972); (b) L. G. Piper, J. E. Velazco, and D. W. Setser, *J. Chem. Phys.* **58**, 3323 (1973); (c) J. E. Velazco and D. W. Setser, *Chem. Phys. Lett.* **25**, 197 (1974).
- ³L. G. Piper, *Chem. Phys. Lett.* **28**, 276 (1974).
- ⁴(a) J. E. Velazco and D. W. Setser, *J. Chem. Phys.* **62**, 1990 (1975); (b) J. E. Velazco and D. W. Setser, *IEEE J. Quantum Electron.* **QE-11**, 708 (1975).
- ⁵O. P. Bochkova, *Opt. Spectrosc.* **28**, 88 (1970).
- ⁶D. H. Winicur and J. L. Fraites, *J. Chem. Phys.* (to be published).
- ⁷(a) V. Kaufman and C. J. Humphries, *J. Opt. Soc. Am.* **59**, 1614 (1969); (b) W. L. Wiese, M. W. Smith, and B. M. Miles, *Natl. Stand. Ref. Data Ser. Natl. Bur. Stand.* **22**, (1969); C. E. Moore, *Natl. Bur. Stand. (U. S.) Circ.* **467**, (1952).
- ⁸P. W. Murphy, *J. Opt. Soc. Am.* **58**, 1200 (1968).
- ⁹A. Perry-Thorne and J. E. Chamberlain, *Proc. Phys. Soc. London* **82**, 133 (1963).
- ¹⁰D. A. Landman and R. Dobrin, *Phys. Rev. A* **8**, 1868 (1973).
- ¹¹(a) E. Ellis and N. D. Twiddy, *J. Phys. B* **2**, 1366 (1969); (b) L. G. Piper (unpublished work); (c) A. V. Phelps and J. P. Molnar, *Phys. Rev.* **89**, 1202 (1953); (d) A. H. Futch and F. A. Grant, *Phys. Rev.* **104**, 356 (1956); (e) J. LeCalve and M. Bourene, *J. Chem. Phys.* **58**, 1446 (1973); (f) N. Sadeghi, *Colloq. Nat. Phys. Coll. Atom. Electron.*, IVth, Brest (1970); (g) W. Wieme and J. Wieme-Lenaerts, *Phys. Lett. A* **47**, 37 (1974).
- ¹²For a more detailed explanation of the absorption of resonance radiation and of the two layer model, see (a) A. C. G. Michell and M. W. Zemansky, *Resonance Radiation and Excited Atoms* (Cambridge U. P., London, 1971); (b) F. Kaufman and D. A. Parkes, *Trans. Faraday Soc.* **66**, 1579 (1970); (c) P. P. Bemand and M. A. A. Clyne, *J. Chem. Soc. Faraday Trans.* **2** **69**, 1643 (1973).
- ¹³J. Geiger, *Phys. Lett. A* **33**, 351 (1970).
- ¹⁴R. Turner, *Phys. Rev. Sect. A* **140**, 426 (1965).
- ¹⁵D. N. Stacey (private communication to J. Geiger, Ref. 14).
- ¹⁶J. M. Vaughan, *Phys. Rev.* **166**, 13 (1968).
- ¹⁷P. R. Berman and W. E. Lamb, Jr., *Phys. Rev. Sect. A* **187**, 221 (1969).
- ¹⁸P. M. Griffin and J. W. Hutcherson, *J. Opt. Soc. Am.* **59**, 1607 (1962).
- ¹⁹J. W. Hutcherson and P. M. Griffin, *J. Opt. Soc. Am.* **63**, 338 (1973).
- ²⁰P. G. Wilkinson, *J. Quant. Spectrosc. Radiat. Transfer* **5**, 503 (1965).
- ²¹G. I. Chashchina and E. Y. Schreider, *Opt. Spectrosc.* **20**, 283 (1966).
- ²²(a) H. S. W. Massey, E. H. S. Burhop, and H. B. Gilbody, *Electronic and Ionic Impact Phenomena* (Clarendon, Oxford, 1971), 2nd ed., Vol. II, p. 1868 (1971); (b) See also Ref. 2b and the references cited therein.
- ²³C. F. Melius and W. A. Goddard III, *Phys. Rev. A* **10**, 1541 (1974).
- ²⁴T. Nenner, *Entropie* **42**, 142 (1971).
- ²⁵D. H. Winicur and J. L. Fraites, *J. Chem. Phys.* **62**, 63 (1975).
- ²⁶J. M. Vaughan and G. Smith, *Phys. Rev.* **166**, 17 (1968).
- ²⁷These are average values obtained from collision broadening and shift at two temperatures based upon the theory described by W. R. Hindmarsh, A. D. Petford, and G. Smith, *Proc. R. Soc. London Ser. A* **297**, 296 (1967). Vaughn and Smith²⁶ list $\Delta C_6 = 2.45 \times 10^{-58} \text{ erg} \cdot \text{cm}^6$, but this value is not compatible with the experimental results as interpreted by their theory.
- ²⁸E. V. Nikifarov and L. E. Scherba, *Opt. Spectrosc.* **32**, 567 (1972).
- ²⁹R. W. Molof, H. L. Schwartz, T. M. Miller, and B. Bederson, *Phys. Rev. A* **10**, 1131 (1974).
- ³⁰(a) M. S. Child, *Discuss. Faraday Soc.* **53**, 18 (1972) and references therein; (b) E. E. Nikitin, in *Chemische Elementarprozesse*, edited by H. Hartman (Springer, Berlin, 1968), pp. 43-77; (c) N. F. Mott and H. S. W. Massey, *The Theory of Atomic Collisions* (Oxford U. P., Oxford, 1965), pp. 353, 804.
- ³¹Y. Tanaka, K. Yoshino, and D. E. Freeman, *J. Chem. Phys.* **59**, 5160 (1973).
- ³²R. Turner, *Phys. Rev.* **158**, 121 (1967).
- ³³P. R. Timpson and J. M. Anderson, *Can. J. Phys.* **48**, 1817 (1970).
- ³⁴W. Wieme, *J. Phys. B* **7**, 850 (1974).
- ³⁵The decay of $\text{Xe}(^3P_2)$ in Ar shows normal rate constants,¹¹ see Ref. 4b.
- ³⁶M. F. Golde and B. A. Thrush, *Chem. Phys. Lett.* **29**, 486 (1974).